Theor Chem Acc (2011) 130:161–173
DOI 10.1007/s00214-011-0949-1

REGULAR ARTICLE

Photophysical properties and vibrational structure of ladder-type penta *p*-phenylene and carbazole derivatives based on SAC-CI calculations

Potjaman Poolmee · Masahiro Ehara · Hiroshi Nakatsuji

Received: 1 March 2011 / Accepted: 20 April 2011 / Published online: 7 May 2011

Abstract The π-conjugated ladder-type molecules constitute an attractive field of organic photoactive materials. In this work, the photophysical properties of ladder-type penta-*p*-phenylene (LPP) and carbazole derivatives (bisindenocarbazole and diindolocarbazole) have been investigated theoretically using the symmetry-adapted cluster-configuration interaction (SAC-CI) method. The equilibrium geometries in the ground (S_0) and first excited (S_1) states were calculated to be planar, and the excitation is delocalized over the molecules. SAC-CI/DZP calculations have been applied to the absorption and emission spectra of these molecules. The absorption spectra were well reproduced in both peak positions and the shape of the absorption bands. The strong absorption is attributed to the highest occupied molecular orbital to the lowest unoccupied molecular orbital (H–L) transition; however, in carbazoles, the H–1→L transition is located below the H–L transition. The vibrational structure in the S_0–S_1 absorption band of LPP was analyzed by calculating the Franck–Condon (FC) factors based on the potential energy surfaces (PESs) along the normal coordinates that are relevant to the geometry change. The vibrational structure was well reproduced by the theoretical simulation. The C–C stretching mode dominantly contributes to the vibrational structure, while the breathing motion of the molecular frame does not influence the structure. The emission energies calculated by the SAC-CI method also agree well with the experimental values. The vibrational structure in the fluorescence band was also examined by the FC analysis; the theoretical spectrum is satisfactory for the two carbazoles, while the 0–0 transition is overestimated in LPP. In diindolocarbazole, the S_2 state has a large oscillator strength, while the S_1 state has a small oscillator strength.

Keywords Excited states · Ladder-type π-conjugated molecule · SAC-CI · Vibrational structure

Dedicated to Professor Shigeru Nagase on the occasion of his 65th birthday and published as part of the Nagase Festschrift Issue.

P. Poolmee
Department of Chemistry, Faculty of Liberal Arts and Science, Kasetsart University, Kamphaeng Saen, Nakhon Pathom 73140, Thailand

M. Ehara (✉)
Research Center of Computational Science, Institute for Molecular Science, 38-Nishigo-Naka, Myodaiji, Okazaki 444-8585, Japan
e-mail: ehara@ims.ac.jp

H. Nakatsuji
Quantum Chemistry Research Institute, Goryo Oohara 1-36, Nishikyo-ku, Kyoto 615-8245, Japan

H. Nakatsuji
JST, CREST, Sanboncho-5, Chiyoda-ku, Tokyo 102-0075, Japan

1 Introduction

The application of quantum chemistry to large systems has seen major developments and is recognized as one of the powerful tools in nanoscale science and chemistry. Professor Shigeru Nagase has significantly contributed to theoretical investigations of nanoscale systems as well as to theoretical development in this field, in particular to fullerene chemistry, and established the "*interplay between theory and experiment*" [1]. This achievement certainly accelerates investigations in nanoscale science and chemistry and ensures the contribution of quantum chemistry to further development of this field.

Organic photoactive and electroactive materials are very attractive because of their good mechanical properties, low cost processing, and their tunable electrical and optical properties through structural modifications. In the particular case of conjugated ladder-type molecules, these coplanar building units are extremely interesting because of a combination of desirable properties, such as good molecular packing, thermal stability, and charge carrier mobility. The first conjugated ladder polymer (ladder poly-*p*-phenylene) (LPPP) was prepared by Scherf and Müllen in 1991 [2]. Since then, many publications [3–6] have appeared, dealing with their synthesis, physical properties, and applications in photonics and optics. Besides the ladder polymers of LPPP type, representatives of a second class of aromatic, conjugated ladder polymers were first developed by Chmil and Scherf [7, 8] in 1993. Subsequently, many researchers have been interested in various types of conjugated ladder-type molecules [9–13].

Among the π-conjugated ladder-type molecules, the poly-phenylenes and carbazole derivatives are of special interest because of their luminescence and conducting properties. The photophysical properties of LPPP have been experimentally investigated in detail by Romanovskii et al. [14]. The absorption and delayed fluorescence/phosphorescence spectra of LPPP oligomers were observed as well as those of ladder-type penta-*p*-phenylene (LPP) [14]. The optical properties of carbazole molecules have also been extensively studied. Sonntag et al. synthesized five new bisindenocarbazoles with some alkyl substituents and investigated their photophysical and electrochemical properties [15]. However, reliable theoretical calculations and assignment have not been performed for the excited states of LPP and bisindenocarbazole. Wakim et al. synthesized the diindolocarbazoles with C_8H_{17} substituents and reported the absorption spectrum [16]. Belletête et al. intensively studied the photophysical properties of some diindolocarbazoles experimentally and theoretically. They analyzed the molecular structures and photophysical properties using density functional theory (DFT) and time-dependent (TD) DFT calculations [17–19]. The intensity ratio of the absorption peaks, however, needs to be further examined and solved for reliable assignments. The system has relatively large π-conjugation, and the TDDFT computations may need a functional with long-range correction.

Quantum chemical calculation is now recognized as a useful tool to investigate the relation between the electronic structure and optical properties of π-conjugated materials. The results from the theoretical calculations can potentially allow us to perform fine-tuning of their optical and electronic properties and then to rationalize the synthesis of the most promising materials. In a series of works, we have investigated the photophysical properties of organic light-emitting diodes (OLEDs) [20–22] and photofunctional molecules [23, 24] using the symmetry-adapted cluster-configuration interaction (SAC-CI) method. The SAC [25]/SAC-CI [26, 27] method originally developed in 1978 has been established as an accurate theory for molecular excited states and has been applied to a wide field of chemistry and physics, such as molecular spectroscopy, biological chemistry, and surface photochemistry [28, 29].

In this work, we investigate the photophysical properties and molecular structure of the ladder-type π-conjugated molecules, LPP and two carbazole derivatives (diindolocarbazole and bisindenocarbazole; Fig. 1), which belong to the class of semiconducting organic materials. SAC-CI calculations have been applied to the absorption and fluorescence spectra of the three molecules. The ground- and excited-state molecular structures have been calculated by the B3LYP [30, 31] and CIS [32] methods, respectively. The vibrational structures in the absorption and emission spectra were also investigated by vibrational analysis and the potential energy surfaces (PESs) around the local minima. The vibrational spectra were simulated using the Franck–Condon (FC) approximation with a reduced number of vibrational modes.

2 Computational details

We have calculated the electronic structure and optical properties of the three ladder-type π-conjugated molecules. The ground-state (S_0) geometries of the molecules were optimized using the B3LYP [30, 31]/6-31G(d) [33] method, and these theoretically optimized structures were used for calculations of their vertical excitation energy. To calculate their emission energy, the equilibrium geometries in the first singlet excited state (S_1) of these compounds were optimized using the CIS [32]/6-31G(d) method. It was confirmed by vibrational analysis that all of the equilibrium structures are at true local minima.

The absorption and emission energies were calculated using the direct SAC/SAC-CI singles and doubles (SD)–*R* non-variational method by directly calculating σ-vectors in the core [34]. To calculate the absorption spectra, five excited states of LPP in the C_{2h} structure were solved, and three excited states of carbazole derivatives for each symmetry in C_{2v} structure were computed. The basis sets of the SAC-CI calculations are the double zeta plus one polarization function (DZP) of Huzinaga–Dunning for the C, N, and H atoms [4s2p1d/2s] [35]. The 1s orbitals of the C and N atoms were treated as frozen-core orbitals. The resultant SAC-CI active space of LPP consists of 80 occupied molecular orbitals (MOs) and 251 unoccupied MOs (80 occ. $\times$ 251 unocc.). For bisindenocarbazole and

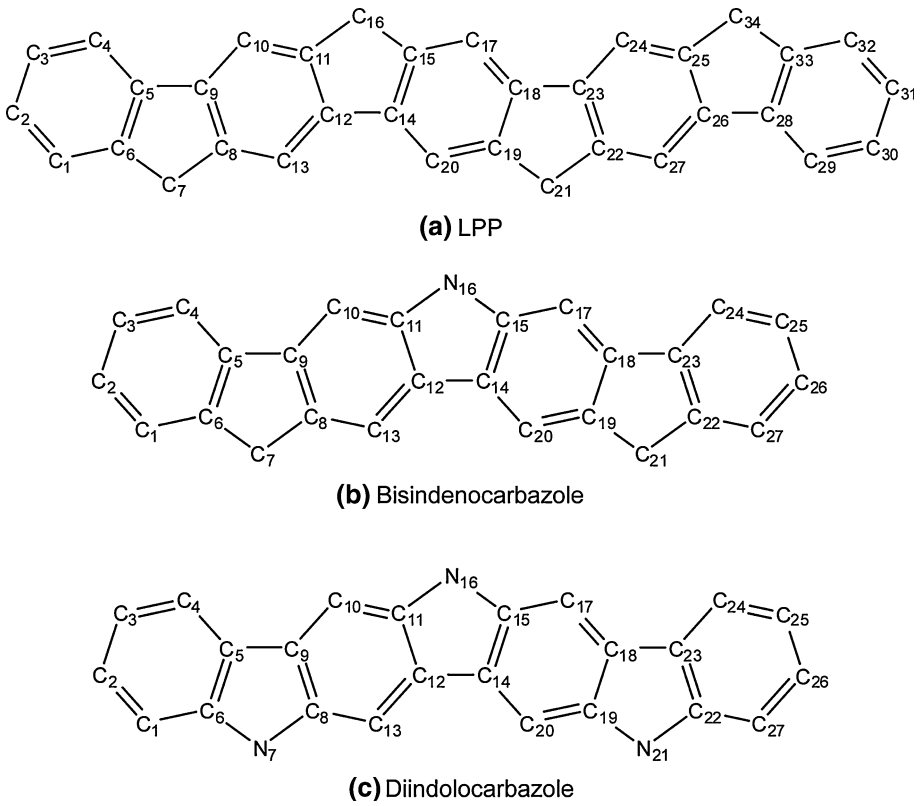

Fig. 1 Molecular structures studied in the present work; **a** LPP (C_{2h}) **b** bisindenocarbazole (C_{2v}) and **c** diindolocarbazole (C_{2v})

diindolocarbazole, the active space is 75 occ. × 250 unocc. MOs and 64 occ. × 198 unocc. MOs, respectively. We focus on the valence-excited states that are relevant for the optical properties of photofunctional molecules. The perturbation-selection technique [36] was adopted to reduce the computational cost, and Level Three accuracy was used. The threshold of the linked terms for the ground state was set to $\lambda_g = 1.0 \times 10^{-6}$. All of the product terms generated by doubles were included in the SAC calculation. For the excited states, the thresholds of the linked doubles were set to $\lambda_e = 1.0 \times 10^{-7}$. All of the product terms generated by the R_1S_2 and R_2S_2 operators were included in the SAC-CI calculations.

To interpret the vibrational structure in the absorption and emission spectra, the vibrational analysis was performed at the equilibrium geometry. The PESs of the S_0 and S_1 states were calculated along some relevant coordinates based on the geometry change between these states, and the vibrational structure was simulated within the FC approximation of the reduced degrees of freedom. To calculate the vibrational structure of the S_0–S_1 absorption spectrum, for example, the S_0 and S_1 PESs were expanded in the normal coordinates $\{q_1, \ldots, q_n\}$ of the S_1 state, and the S_0-state equilibrium geometry was described by the displacement from the S_1-state equilibrium geometry. Then, the $S_0(g)$ and $S_1(e)$ PESs were expanded in the relevant normal coordinates $\{q_1, \ldots, q_n\}$ of the S_1 state as:

$$V_g(q_1, \ldots, q_n) = \sum_{i=1}^{n} \sum_{m=0}^{4} B_{g,\mathrm{im}} \left(q_i - q_{g,i}\right)^m, \tag{1}$$

$$V_e(q_1, \ldots, q_n) = \sum_{i=1}^{n} \sum_{m=0}^{4} B_{e,\mathrm{im}} q_i^m, \tag{2}$$

where $\{q_{g,1}, \ldots, q_{g,n}\}$ is the displacement from the local minimum of the S_0 state from that of the S_1 state and $\{B_{g,\mathrm{im}}\}, \{B_{e,\mathrm{im}}\}$ are expansion coefficients. Note that mode–mode coupling is not considered in the PESs. The DFT(B3LYP)/VDZ and CIS/VDZ calculations were used for the vibrational analysis. The DFT(B3LYP) includes the effect of electron correlation, while CIS does not include it. This difference affects the equilibrium geometries and FC factors. Electron correlation, however, does not affect much on the geometry, and basis set is usually more important. The coefficients $\{B_{g,\mathrm{im}}\}, \{B_{e,\mathrm{im}}\}$ were determined by a least-square fit using the ab initio data. The vibrational wavefunctions of the S_0 and S_1 states were calculated with these PESs, and the FC factors were evaluated with these vibrational wavefunctions. The vibrational structure in the emission spectra was also simulated in the same manner, with the coordinates being based on the ground-state normal modes.

Vibrational progressions in absorption/emission spectra usually appear for those coordinates whose structure changes are large between the ground and excited states.

For a large system, however, it is too expensive practically to include the effect of all of the coordinates. Therefore, in the case of absorption, for example, we describe the geometry change by a linear combination of normal modes of the excited state as:

$$\Delta r = \sum_i c_i q_i = \sum_i q_{g,i}, \tag{3}$$

and extract the relevant coordinates that have large coefficients c_i, which are called the weight in the present paper. The coordinates selected in this manner could contribute to the vibrational structure. The numbering of vibrational modes in the present work is given in the increasing order of the vibrational frequencies.

The SAC/SAC-CI calculations were performed using the Gaussian09 suite of programs Revision B.01 [37]. The vibrational wavefunctions were calculated with the MCTDH program package [38].

3 Results and discussion

3.1 Ground- and excited-state geometries

The equilibrium geometries in the S_0 and S_1 states of the three ladder-type π-conjugated molecules were calculated by the B3LYP/6-31G(d) and CIS/6-31G(d) methods, respectively. The structures were confirmed to be local minima; none of the optimized structures exhibited negative eigenvalues of the Hessian matrix. The equilibrium structures are presented for the C–C and C–N bond lengths in Fig. 2; the bond lengths in S_0 are shown with those in S_1 in parentheses. For diindolocarbazoles, Belletête et al. [17, 18] have reported the optimized structures of the ladder oligo(*p*-aniline) in dimer and trimer derivatives with some alkyl substitutions using HF/6-31G(d) and DFT/6-31G(d) calculations. They showed that the structure of the dimer was well reproduced by comparison with the X-ray structure [17].

The present results show that the equilibrium structures are planar in both the ground and excited states of all three molecules, which is also expected from the rigid structure of the ladder-type π-conjugated molecules. Comparing the equilibrium structure in the S_0 and S_1 states, the bond lengths show some changes, while the bond angles do not change significantly. The changes in bond length can be interpreted with the MOs involved in the transitions. These relevant MOs are shown in Fig. 3 for LPP, bisindenocarbazole, and diindolocarbazole.

The S_1 state of LPP is characterized as the transition from highest occupied MO (HOMO) to lowest unoccupied MO (LUMO). Both MOs are of π-type and spread over the whole conjugated backbone. Interestingly, the HOMO distribution of diindolocarbazole is different from LPP and bisindenocarbazole. It can be understood from their carbazole-like character [17]. The HOMO of LPP is in phase across *r*(4,5), *r*(5,6), *r*(8,9), *r*(9,10), *r*(11,12), *r*(12,13), *r*(14,15), *r*(14,20), and their symmetrically equivalent bonds, while the LUMO is in antiphase for these bonds. As expected, these bonds are lengthened, as presented in Fig. 2. On the other hand, the HOMO of LPP is in antiphase across *r*(5,9), *r*(8,13), *r*(10,11), *r*(12,14), *r*(15,17), *r*(19,20), and their symmetrically equivalent bonds, whereas the LUMO is in phase for these bonds, and therefore, a contraction of these bonds occurs. This trend is also valid in the two carbazoles depending on the excitation character. It is also noted that the inter-ring distances decrease in the S_1 state, because the HOMO has inter-ring antibonding character between the phenylene subunits, while the LUMO has inter-ring bonding character. Thus, the molecule shows a quinoid structure in the excited state. The inter-ring distance of the carbazoles ($\sim$1.449 Å) is shorter than that of LPP ($\sim$1.467 Å) at the *N*-substituted points because the C–N bond is much shorter than the C–C bond. This also has an influence on the excitation characters of these molecules. For diindolocarbazole, the present calculations well reproduce the previous DFT(B3LYP)/6-31G(d) calculation for the trimer, for which no X-ray structure has been reported [17].

3.2 Absorption spectra

The absorption spectra of LPP, diindolocarbazole, and bisindenocarbazole were calculated by the SAC-CI method at the B3LYP/DZP ground-state geometry. The results of absorption energies, oscillator strength, and transition characters are summarized in the tables together with the available experimental values. The calculated absorption spectra are also compared with the experimental spectra for these molecules. For LPP, the absorption spectrum has a clear vibrational progression, and therefore, we also calculated the FC factors to explain the spectrum.

3.2.1 Absorption spectrum of ladder-type penta-p-phenylene

The absorption and fluorescence spectra of ladder-type alkyl-substituted pentaphenylene were observed as one of the methyl-substituted poly-phenylenes (MeLPPP) [14], while the detailed assignment of these spectra has not been achieved so far. To interpret the absorption spectrum of LPP, the SAC-CI/DZP calculations were performed at the ground-state geometry. The results are compiled in Table 1 with the experimental values. The calculated absorption spectrum is compared with the experimental spectrum in Fig. 4. The observed spectrum shows vibrational

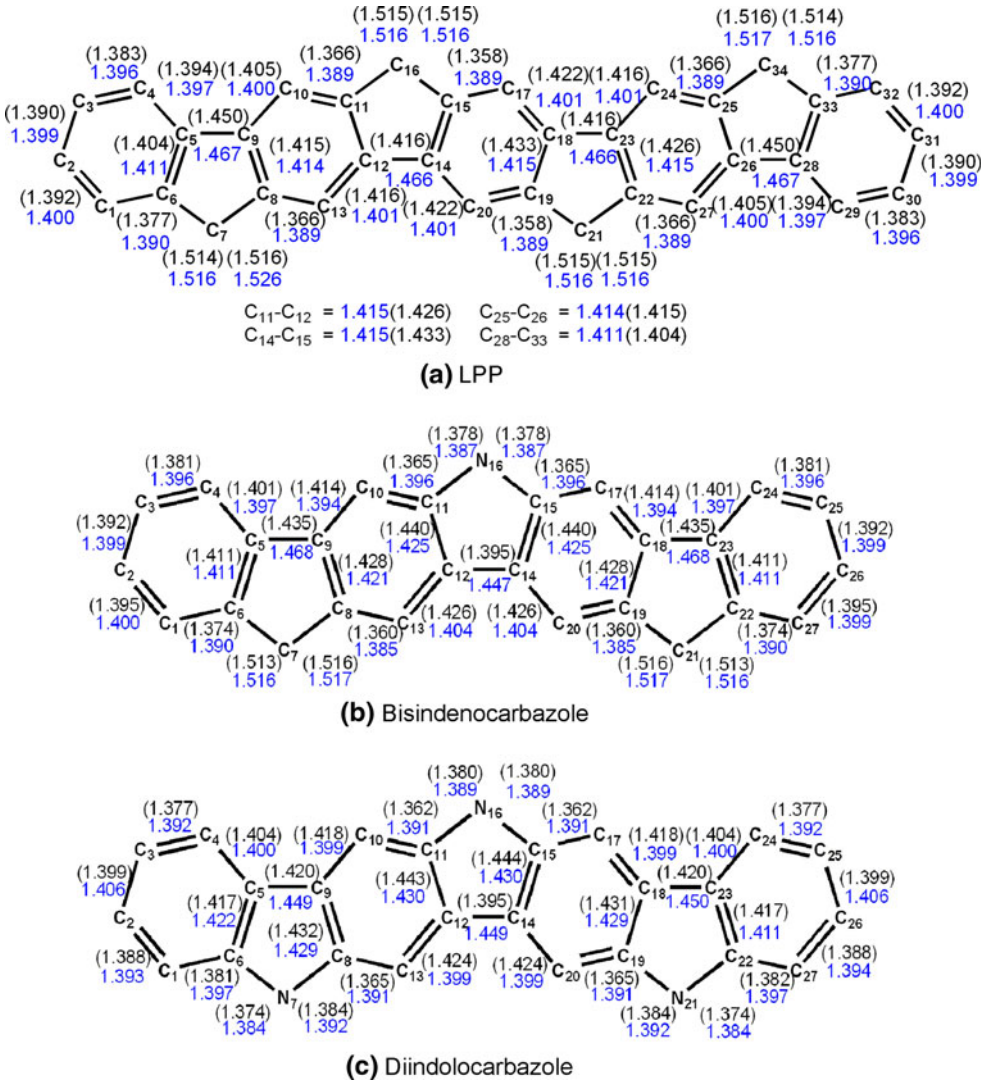

Fig. 2 Bond lengths (in Å) of the S_0 and S_1 (in parenthesis)-state geometries; **a** LPP, **b** bisindenocarbazole and **c** diindolocarbazole

progressions starting from ~3.22 eV (26,000 cm^{-1}). The present SAC-CI calculation of LPP provided the $1B_u$ state of the HOMO → LUMO (H–L) transition at 3.19 eV with the oscillator strength of $f = 1.51$, which shows excellent agreement with the experimental spectrum. The higher $2B_u$ state of the H → L + 2 transition was calculated at 3.80 eV with non-negligible oscillator strength. This $2B_u$ state overlaps with the vibrational progression of the $1B_u$ state as seen in Fig. 4.

To interpret the vibrational structure in the absorption spectrum of LPP, the geometry relaxation in the S_0–S_1 transition was analyzed. The geometry changes are described on the basis of the normal modes in the S_1 state, and the relevant coordinates with weights larger than 0.05 are shown in Table 2. The normal coordinates were obtained by the vibrational analysis using the CIS/VDZ calculations. The totally symmetric modes of q_7 ($v = 126$ cm^{-1}), q_9 ($v = 154$ cm^{-1}), q_{18} ($v = 327$ cm^{-1}), q_{140} ($v = 1{,}808$ cm^{-1}), and q_{77} ($v = 1{,}117$ cm^{-1}) make a contribution, some of which are shown in Fig. 5. The low-frequency modes such as q_7, q_9, and q_{18}, however, do not contribute to the vibrational progression from this one-dimensional analysis; that is, the (0–0) transition is dominant. These low-frequency modes correspond to the breathing motion of the molecular frame. Therefore, we performed a two-dimensional (2-D) PES analysis based on the q_{140} and q_{77} coordinates. The vibrational mode of q_{140} is the C–C stretching motion, as shown in Fig. 5. The 2-D vibrational wavefunctions and the FC factors of the S_0–S_1 transition were calculated based on the 2-D PESs. The calculated FC factors reproduced the experimental vibrational structure well, as shown in Fig. 4a and b, although the calculated vibrational spacing was larger than the experimental vibrational progression because of the crude quality of the CIS/VDZ calculation. The vibrational progression of the q_{140} mode is dominant, and the contribution of the q_{77} mode is rather small in this case.

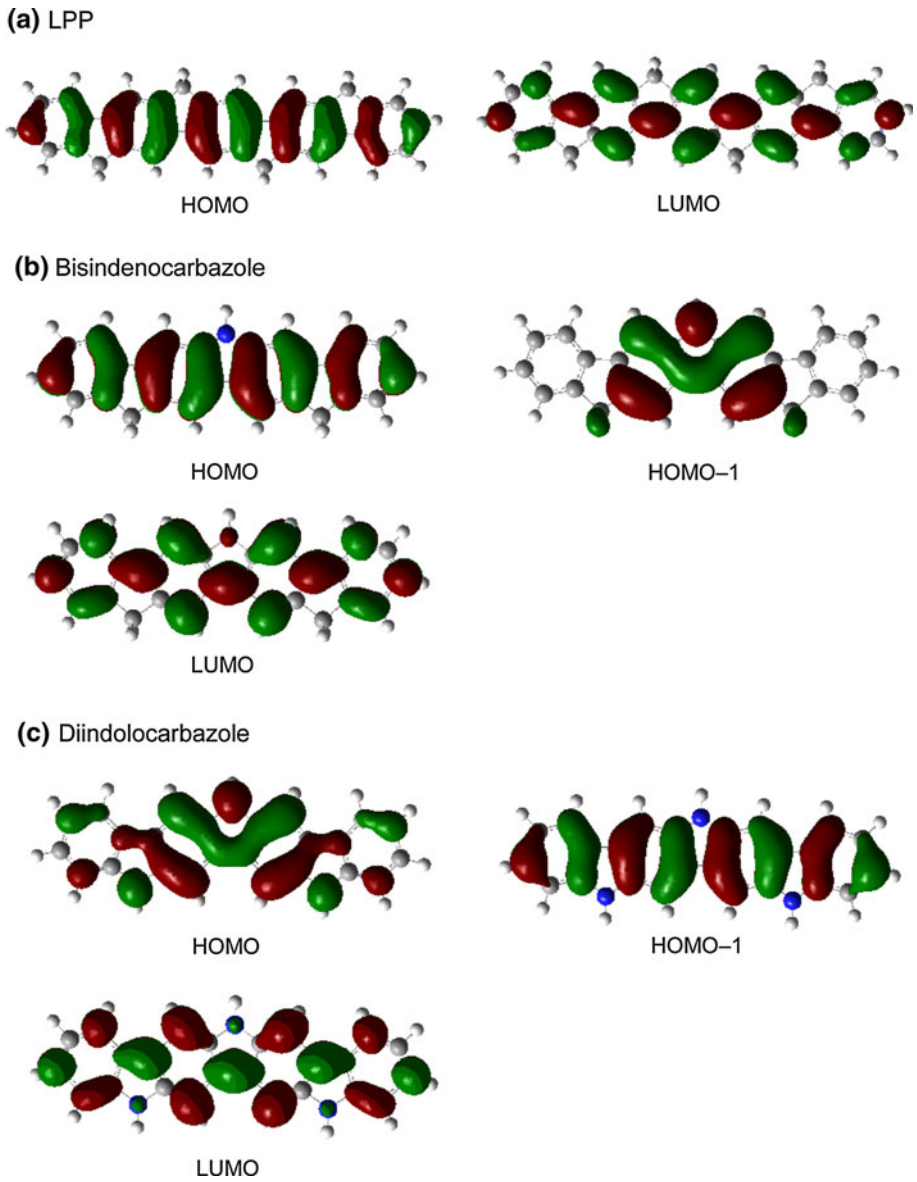

Fig. 3 Relevant MOs in the valence excitations of **a** LPP, **b** bisindenocarbazole and **c** diindolocarbazole

Table 1 Absorption energy (ΔE/eV, cm^{-1}), oscillator strength (f), and transition character of the singlet excited states of LPP calculated by SAC-CI

SAC-CI				Expt.[a]
State	Transition character	ΔE, eV (cm^{-1})	f	ΔE, eV (cm^{-1})
$1B_u$	0.88 (H→L)	3.19 (25,700)	1.505	~ 3.22 (26,000)
$2B_u$	0.78 (H→L+2)	3.80 (30,700)	0.246	
$2A_g$	0.50 (H→L+3)−0.40 (H→L+1)	4.18 (33,700)	0.000	
$3B_u$	0.52 (H−2→L)+0.36 (H→L+4)	4.39 (35,400)	0.006	
$3A_g$	0.53 (H−1→L)+0.51 (H→L+1)	4.74 (38,200)	0.000	

[a] Ref. [14]

3.2.2 *Absorption spectrum of bisindenocarbazole*

Sonntag et al. have synthesized some derivatives of bisindenocarbazoles with different alkyl substituents and performed a characterization, including their optical properties [15]. They found that a change in the alkyl side chain has no significant influence on the absorption spectrum of the bisindenocarbazole chromophore. Thus,

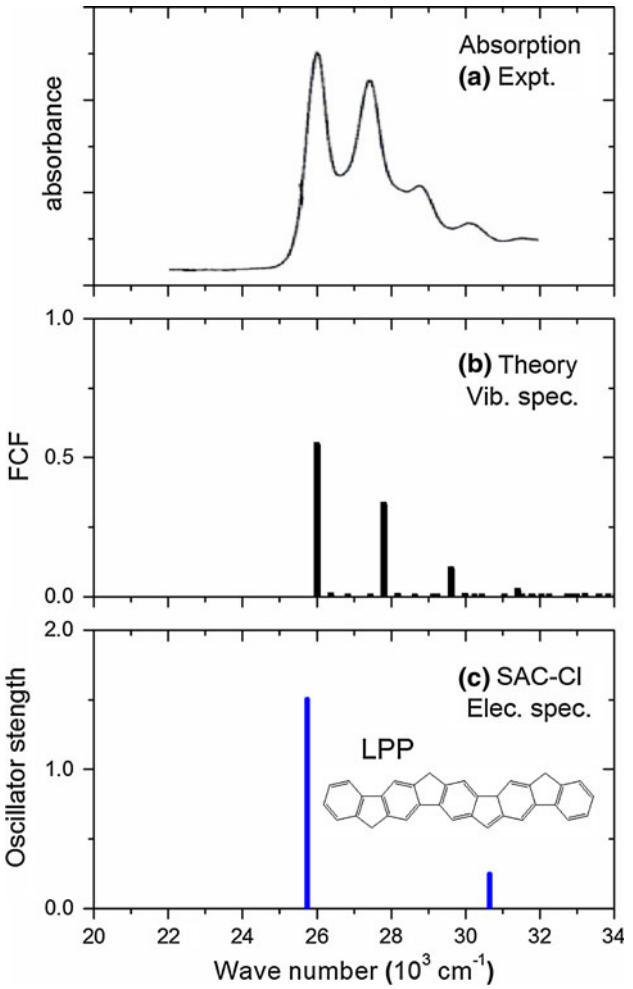

Fig. 4 **a** Experimental absorption spectrum [14], **b** vibrational structure computed with the CIS/B3LYP 2D PESs, and **c** SAC-CI absorption spectrum of LPP. In the vibrational spectrum (**b**), peaks are shifted to fit the 0–0 transition

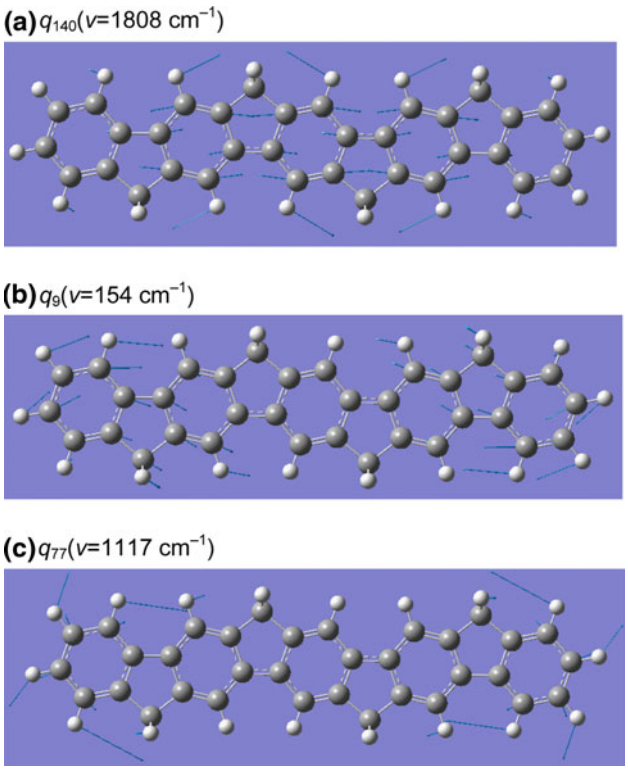

Fig. 5 Relevant vibrational modes in the absorption spectrum and geometry relaxation in S_0–S_1 transition of LPP

similar experimental UV–vis spectra were obtained for the derivatives, as shown in Fig. 6. To interpret the absorption spectrum, the excited states of bisindenocarbazole were calculated using the SAC–CI/DZP method at the ground-state geometry. The results of the vertical absorption for this molecule are summarized in Table 3 along with the experimental values [15]. The calculated absorption spectrum without vibrational levels is compared with the experimental absorption spectrum [15] in Fig. 6.

The experimental spectrum has two strong peaks at 3.35 and 3.54 eV (380 and 350 nm), which originate in different electronic states. The present calculation provided the $2A_1$ and $1B_2$ states at 3.48 and 3.53 eV (356 and 352 nm), respectively, with the oscillator strength of the latter state being large. For these absorptions, a vibrational progression or FC envelope is also expected in the higher energy region of these peaks based on the vibrational analysis. The

Table 2 Relevant vibrational modes in the geometry changes in the S_0–S_1 transition (absorption) with vibrational frequency and weight

LPP			Bisindenocarbazole			Diindolocarbazole		
Mode	ν (cm^{-1})	Weight	Mode	ν (cm^{-1})	Weight	Mode	ν (cm^{-1})	Weight
q_9	154	0.46	q_8	185	0.39	q_8	185	0.40
q_7	126	0.23	q_{14}	328	0.11	q_{13}	332	0.12
q_{18}	327	0.11	q_4	83	0.10	q_4	84	0.12
q_{140}	1,808	0.06	q_{109}	1,807	0.05	q_{37}	769	0.05
q_{77}	1,117	0.05	q_{30}	645	0.05	q_{105}	1,813	0.05
			q_{60}	1,114	0.05			

The vibrational modes are based on the normal coordinates of the S_1 state. Weight is defined in Eq. 3

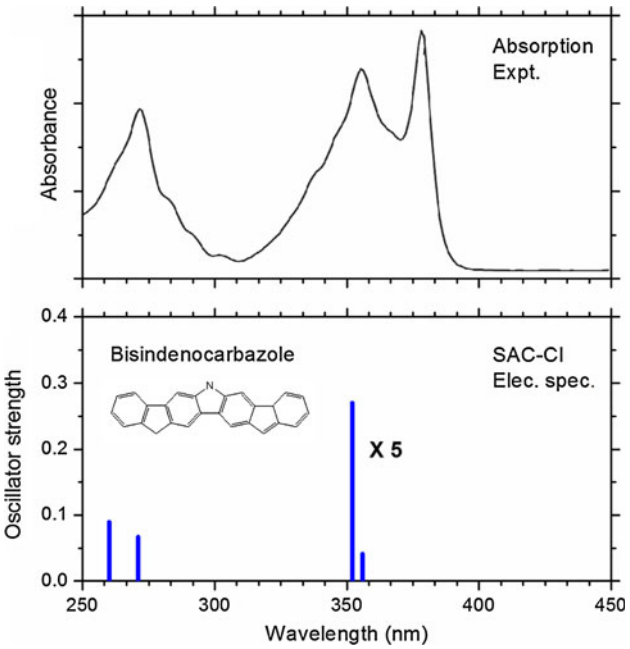

Fig. 6 SAC-CI absorption spectrum of bisindenocarbazole compared with the experimental spectrum [15]

geometry relaxation in the XA_1–$1B_2$ transition was also analyzed as in LPP, and the results are summarized in Table 2. A vibrational progression due to the q_{109} ($v = 1{,}807\ \mathrm{cm}^{-1}$) mode is expected. The observed peak centered at around 4.59 eV (270 nm) is assigned to the $2B_2$ and $3B_2$ states calculated at 4.57 and 4.78 eV (271 and 260 nm), respectively. These transitions have considerable oscillator strengths of $f = 0.067$ and 0.089.

3.2.3 Absorption spectrum of diindolocarbazole

The alkyl-substituted diindolocarbazoles were synthesized, and the UV–vis absorption spectrum of a derivative with C_8H_{17} substitution was observed by Wakim et al. [16]. The series of the ladder oligo(*p*-anilines), dimer, and trimers was also investigated by Belletête et al. [17, 18]. They performed a detailed analysis of the molecular structures and absorption spectra of these derivatives using HF, DFT(B3LYP)/6-31G(d), and TDDFT(B3LYP)/6-31G(d) calculations. The result obtained from TDDFT/6-31G(d) shows that the $S_1 \leftarrow S_0$ transition (H–L) is weakly allowed, whereas the $S_2 \leftarrow S_0$ transition (H–1→L) possesses a large oscillator strength. We have investigated the excited states of the diindolocarbazole using SAC-CI/DZP calculations. The SAC-CI results of the vertical absorption of diindolocarbazole are summarized in Table 4, and the calculated electronic spectrum is compared with the experimental absorption spectrum [16] in Fig. 7.

In the low-energy region, two weak absorption peaks were observed at 2.66 and 2.82 eV (466 and 439 nm). The $2A_1$ state was calculated at 2.84 eV (437 nm) with the small oscillator strength of $f = 0.07$, and no other electronic states were obtained in this energy region. The two peaks in the experimental spectra are thus assigned to the vibrational structure of the $2A_1$ state. This result supports the previous TDDFT calculation [17]. The strong peaks were observed at 3.28 and 3.48 eV (378 and 356 nm), and the intensity of the peak at 3.28 eV is larger than that of the peak at 3.48 eV. Based on the peak shape, these are not due to a single electronic state. Accordingly, the present SAC-CI calculation provided the $1B_2$ and $2B_2$ states at 3.47 and 3.68 eV (358 and 337 nm) with oscillator strengths of $f = 1.165$ and 0.211, respectively. The previous TDDFT calculations, on the other hand, gave a different intensity ratio for these peaks [17]; this may be due to the fact that a long-range correction was not included in the functional. In the higher energy region, the $3B_2$ state was calculated at 4.77 eV with $f = 0.514$. Unfortunately, no experimental spectrum was reported in this energy region.

Table 3 Absorption energy (ΔE/eV, nm), oscillator strength (f), and transition character of the singlet excited states of bisindenocarbazole calculated by SAC-CI

SAC-CI				Expt.[a]
State	Transition character	ΔE, eV (nm)	f	ΔE, eV (nm)
$2A_1$	0.84 (H−1→L)	3.48 (356)	0.041	~ 3.35 (380)
$3A_1$	0.62 (H→L+2) + 0.46 (H→L+1)	5.05 (245)	0.001	
$4A_1$	0.47 (H→L+1)	4.47 (278)	0.007	
$1A_2$	0.87 (H−9→L)	7.04 (176)	–	
$2A_2$	0.91 (H→L+8)	7.38 (168)	–	
$3A_2$	0.75 (H−12→L)	7.31 (170)	–	
$1B_1$	0.88 (H−1→L+8)	6.95 (178)	0.001	
$2B_1$	0.74 (H−10→L)	7.07 (175)	0.002	
$3B_1$	0.69 (H−13→L)	7.32 (169)	0.000	
$1B_2$	0.89 (H→L)	3.53 (352)	1.355	~ 3.54 (350)
$2B_2$	0.63 (H→L+3)	4.57 (271)	0.067	~ 4.59 (270)
$3B_2$	0.46 (H→L+5)	4.78 (260)	0.089	

[a] Ref. [15]

Table 4 Absorption energy (ΔE/eV, nm), oscillator strength (f), and transition character of the singlet excited states of diindolocarbazole calculated by SAC-CI

SAC-CI				Expt.[a]
State	Transition character	ΔE, eV (nm)	f	ΔE, eV (nm)
$2A_1$	0.85 (H−1→L)	2.84 (437)	0.070	2.66 (466) 2.82 (439)
$3A_1$	0.56 (H−3→L)−0.38 (H−2→L+1)	4.37 (284)	0.013	
$4A_1$	0.53 (H→L+1)+0.47 (H−1→L+2)	4.89 (253)	0.000	
$1A_2$	0.78 (H−1→L+9)	6.66 (186)	–	
$2A_2$	0.83 (H−1→L+12)	7.49 (166)	–	
$3A_2$	0.88 (H→L+8)	7.29 (170)	–	
$1B_1$	0.83 (H−1→L+8)	6.37 (195)	0.003	
$2B_1$	0.74 (H−1→L+10)	6.77 (183)	0.001	
$3B_1$	0.89 (H−1→L+11)	7.37 (168)	0.001	
$1B_2$	0.83 (H→L)	3.47 (358)	1.165	3.28 (378)
$2B_2$	0.69 (H−2→L)	3.68 (337)	0.211	3.48 (356)
$3B_2$	0.61 (H−1→L+1)+0.46 (H−1→L+3)	4.77 (260)	0.514	

[a] Ref. [16], compound substituted with $-C_8H_{17}$ at N

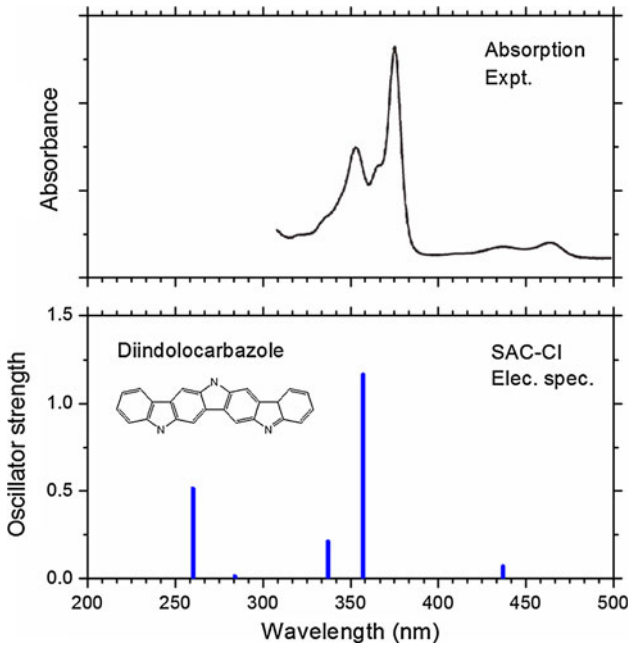

Fig. 7 SAC-CI absorption spectrum of diindolocarbazole compared with the experimental spectrum [16]

The geometry relaxation in the XA_1–$1B_2$ transition was also analyzed with the normal coordinates of the $1B_2$ state. The results are summarized in Table 2. As in LPP, a contribution from the C–C bond-stretching motion of q_{105} ($v = 1{,}813$ cm^{-1}) was found as well as the breathing motions of the molecular frame, such as q_8 ($v = 185$ cm^{-1}), q_{13} ($v = 332$ cm^{-1}), and q_4 ($v = 84$ cm^{-1}). This vibrational q_{105} mode produces the vibrational structure or the FC envelope in the strong band in the energy range of 350–380 nm.

Comparing the carbazole molecule [39] with the diindolocarbazole, the excitation energy of S_1 in carbazole calculated by TDDFT–LDA was 3.66 eV [expt.: 3.62 eV (crystal) and 3.81 eV (vapor)], which is higher than that of diindolocarbazole (3.47 eV). This is attributed to the fact that the molecular structure of diindolocarbazole has a long π-conjugation and a more planar structure. In the case of the polymer, the excitation energy of S_1 in poly(2,7-carbazole) obtained from the absorption spectra (3.24 eV or 383 nm [40]) is also higher than that of polydiindolocarbazole (2.92 eV or 425 nm [41]).

3.3 Emission spectra

The fluorescence spectra of alkyl-substituted derivatives of these three molecules have been observed experimentally [14, 15, 19]. The lowest excited-state geometries of the three molecules were calculated using CIS/6-31G(d), and the vertical emission energies were calculated using the SAC-CI/DZP method. The results for the three molecules are summarized in Table 5 with the experimental values [14, 15, 19]. The vibrational FC factors were also examined, as in the absorption spectrum. The resultant theoretical spectra are compared with the experimental spectra in Figs. 8, 9, and 10 for LPP, bisindenocarbazole, and diindolocarbazole, respectively.

The emission energy of LPP was calculated to be 2.83 eV (22,800 cm^{-1}). In the experimental spectrum, vibrational structure exists and the second peak at 2.97 eV (24,000 cm^{-1}) seems to be close to the vertical emission energy because it has the largest intensity. To understand the vibrational structure, we performed an analysis of the geometry change based on the ground-state normal modes. The results of the relevant coordinates are summarized in

Table 5 Emission energy (ΔE, eV), oscillator strength (f), and transition character of the singlet excited states of LPP, bisindenocarbazole, and diindolocarbazole calculated by SAC-CI

SAC-CI				Expt.
Molecule	Transition character	ΔE/eV	f	ΔE/eV
LPP				
$1B_u$	0.92 (H→L)	2.83 (22,800 cm^{-1})	1.661	~ 2.97 (24,000 cm^{-1})[a]
Bisindenocarbazole				
$1B_2$	0.91 (H→L)	3.19 (388 nm)	1.490	~ 3.19 (388 nm)[b]
Diindolocarbazole				
$2A_1$	0.90 (H−1→L)	2.42 (19,500 cm^{-1})	0.065	~ 2.68 (21,600 cm^{-1})[c]
$1B_2$	0.92 (H→L)	2.89 (23,300 cm^{-1})	1.292	

[a] Ref. [14], compound substituted with $-C_8H_{17}$ at N

[b] Ref. [15]

[c] Ref. [19]

Table 6. Among the contributed normal coordinates, the totally symmetric modes of q_9 (ν = 144 cm^{-1}), q_7 (ν = 116 cm^{-1}), q_{18} (ν = 303 cm^{-1}), q_{81} (ν = 1,045 cm^{-1}), q_{105} (ν = 1,280 cm^{-1}), and q_{138} (ν = 1,665 cm^{-1}) make a significant contribution. The vibrational spectrum of the S_1–S_0 emission was simulated within the FC approximation using the B3LYP, CIS/VDZ 2-D PESs along the q_{105} and q_{138} coordinates. The resultant theoretical spectrum, however, shows that the (0–0) transition has the largest FC factor, while the experimental spectrum has the largest peak for the (0–1) transition, as shown in Fig. 8. This indicates that the geometry changes calculated by CIS/VDZ are not satisfactory.

The emission energy of bisindenocarbazole was calculated as 3.19 eV, which shows excellent agreement with the experimental value of 3.19 eV (388 nm). The observed emission spectrum also has vibrational structure. From the vibrational analysis, the vibrational modes of q_{109} (ν = 1,682 cm^{-1}) and q_{64} (ν = 1,046 cm^{-1}) were found to be relevant coordinates (Table 6), and the vibrational spectrum was simulated with the 2-D PESs along these coordinates. The resultant vibrational structure in the emission spectrum is compared in Fig. 9. The calculated vibrational structure in the S_1–S_0 transition is reasonable compared with the experimental spectrum, although the theoretical spectrum slightly overestimated the FC factors of the (0–0) transition.

Considering the fluorescence of diindolocarbazole, the second excited state, the $1B_2$ (S_2) state whose emission energy was calculated to be 2.89 eV (23,300 cm^{-1}), has the large oscillator strength of f = 1.292. The $2A_1$ (S_1) excited state, however, is located in the lower energy region. The calculated emission energy was 2.42 eV (19,500 cm^{-1}) with the small oscillator strength of f = 0.065. The emission spectrum was observed from the S_1 state with the peak

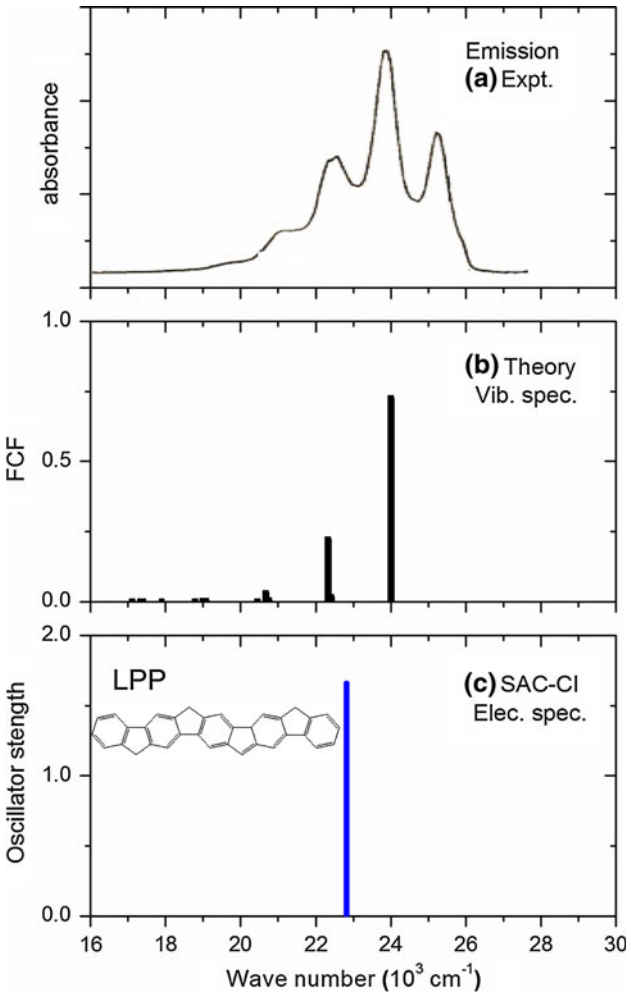

Fig. 8 **a** Experimental emission spectrum [14], **b** vibrational structure computed with 2D B3LYP/CIS PESs, and **c** SAC-CI emission spectrum of LPP. In the vibrational spectrum (**b**), peaks are shifted to fit the 0–0 transition

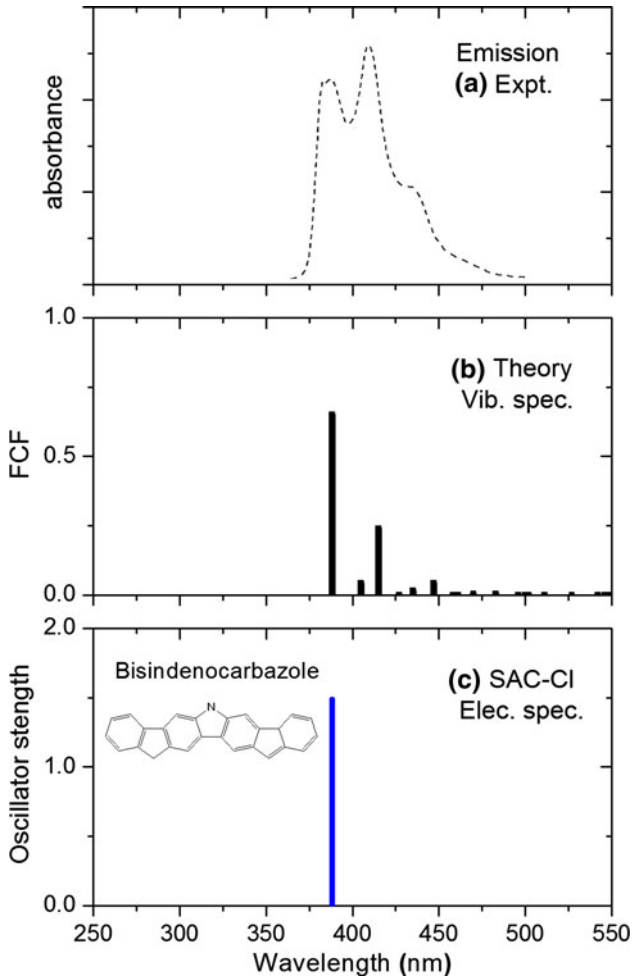

Fig. 9 **a** Experimental emission spectrum [15], **b** vibrational structure computed with 2D B3LYP/CIS PESs, and **c** SAC-CI emission spectrum of bisindenocarbazole. In the vibrational spectrum (**b**), peaks are shifted to fit the 0–0 transition

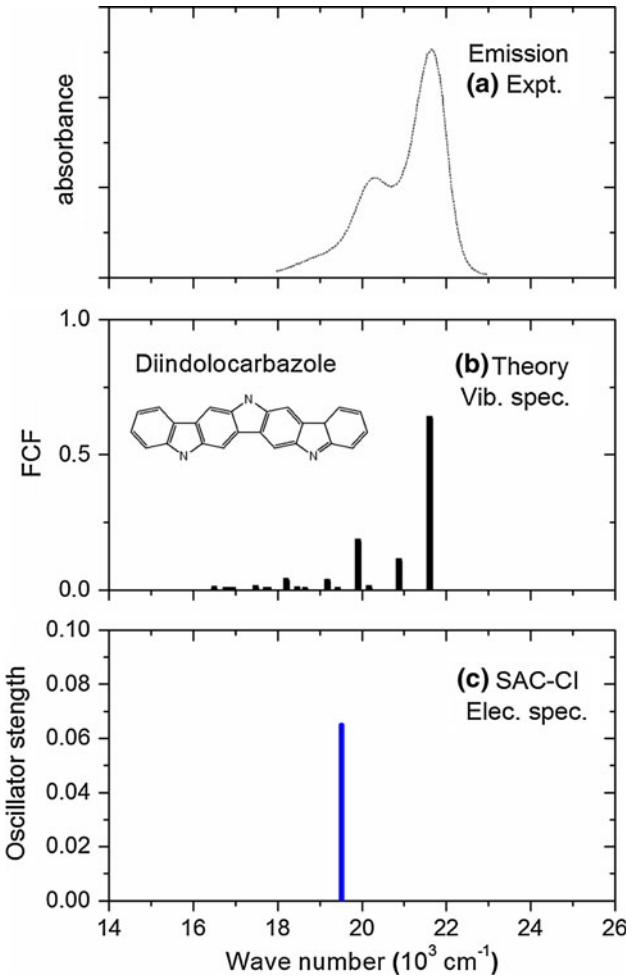

Fig. 10 **a** Experimental emission spectrum [19], **b** vibrational structure computed with 2D B3LYP/CIS PESs, and **c** SAC-CI emission spectrum of diindolocarbazole. In the vibrational spectrum (**b**), peaks are shifted to fit the 0–0 transition

maximum at 2.68 eV (21,600 cm^{-1}) for the trimer of the oligo(*p*-aniline) derivative, TRIMER 2P in their work [19]. In the present study, to interpret the vibrational progression, the FC factors were calculated with the q_{105} (v = 1,691 cm^{-1}) and q_{36} (v = 716 cm^{-1}) modes, whose contributions to the geometry change were large. The theoretical spectrum reproduced the experimental spectrum satisfactorily, as shown in Fig. 10. The vibrational structure is dominantly attributed to the C–C bond-stretching mode (q_{105}), but the contribution from q_{36} is also important. The fluorescence from the S_2 state is expected to be strong, although it may compete with the decay to the S_1 state.

4 Summary

The absorption and emission spectra of LPP, bisindenocarbazole, and diindenocarbazole, which belong to the class of ladder-type π-conjugated molecules, have been investigated by the SAC-CI method. The vibrational structure in the absorption/emission bands was also analyzed based on the vibrational analysis and the PESs around the local minima.

The equilibrium geometries of the S_0 and S_1 states were calculated to be planar in these three ladder-type π-conjugated molecules. The excitation is delocalized over the molecules. Because the molecules have a rigid structure, the bond lengths show some changes, while the bond angles do not change significantly. The interphenylene ring distances decrease in the S_1 state; the HOMO has inter-ring antibonding character among subunits, while the LUMO has inter-ring bonding character. In diindolocarbazole, the HOMO shows a unique carbazole-like character that shows inter-ring bonding character.

The SAC-CI/DZP calculations have been applied to the absorption and emission spectra of the three molecules. The

Table 6 Relevant vibrational modes in the geometry changes in the S_1–S_0 transition (emission) with vibrational frequency and weight

LPP			Bisindenocarbazole			Diindolocarbazole		
Mode	ν (cm^{-1})	Weight	Mode	ν (cm^{-1})	Weight	Mode	ν (cm^{-1})	Weight
q_9	144	0.46	q_8	174	0.39	q_8	175	0.40
q_7	116	0.22	q_{13}	303	0.12	q_{12}	307	0.12
q_{18}	303	0.11	q_3	76	0.10	q_3	78	0.11
q_{81}	1,045	0.05	q_{64}	1,046	0.05	q_{36}	716	0.05
q_{105}	1,280	0.05	q_{109}	1,682	0.05	q_{105}	1,691	0.05
q_{138}	1,665	0.05						

The vibrational modes are based on the normal coordinates of the S_0 state. Weight is defined in Eq. 3

absorption spectra were well reproduced in both the peak positions and the shape of the absorption spectra, and consequently, reliable assignments were achieved. The main absorption with the largest oscillator strength involves the H–L transition; however, in bisindenocarbazole and diindolocarbazole, the H–1→L transition is located below the H–L transition. The vibrational structure in the S_0–S_1 absorption band of LPP was analyzed by calculating the FC factors based on the PESs along the normal coordinates that are relevant in the geometry relaxation. The vibrational structure was well reproduced; the C–C stretching mode dominantly contributes to the vibrational structure, while the breathing motion of the molecular frame does not influence the vibrational structure.

The emission energies calculated by the SAC-CI method also agree well with the experimental values for the three molecules. The vibrational structure in the fluorescence band was also examined by FC analysis. The FC factors of the calculated vibrational structure in the S_1–S_0 transition are reasonable for bisindenocarbazole and diindolocarbazole; however, the 0–0 transition was overestimated for LPP. In diindolocarbazole, the S_2 state has a large oscillator strength, while the S_1 state has a small oscillator strength. Therefore, fluorescence from the S_2 state is expected to be strong, although it may compete with decay to the S_1 state.

Acknowledgments This study was supported by JST–CREST, a Grant–in–Aid for Scientific Research from the Japanese Society for the Promotion of Science (JSPS) and the Ministry of Education, Culture, Sports, Science and Technology (MEXT) of Japan. The computations were partly performed using the Research Center for Computational Science in Okazaki, Japan.

References

1. Akasaka T, Nagase S (2002) Endofullerenes: a new family of carbon clusters. Kluwer, Dordrecht
2. Scherf U, Müllen K (1991) Macromol Chem Rapid Commun 12:489
3. Scherf U, Bohnen A, Müllen K (1992) Macromol Chem 193:1127
4. Grüner J, Wittmann HF, Hamer PJ, Friend RH, Huber J, Scherf U, Müllen K, Moratti SC, Holmes AB (1994) Synth Metal 67:181
5. Köhler A, Grüner J, Friend RH, Müllen K, Scherf U (1995) Chem Phys Lett 243:456
6. Barth S, Bäβler H, Scherf U, Müllen K (1998) Chem Phys Lett 288:147
7. Chmil K, Scherf U (1993) Macromol Chem Rapid Commun 14:217
8. Chmil K, Scherf U (1997) Acta Polym 48:208
9. Chen J-C, Lee T-S, Lin C-H (2008) Chem Eur. J 14:2777
10. Oyaizu K, Iwasaki T, Tsukahara Y, Tsuchida E (2004) Macromolecules 37:1257
11. Leuninger J, Trimpin S, Rädder H-J, Müllen K (2001) Macromol Chem Phys 202:2832
12. Sirringhaus H, Friend RH, Wang C, Leuninger J, Müllen K (1999) J Mater Chem 9:2095
13. Wang H, Schaffner-Hamann C, Marchioni F, Wudl F (2001) Adv Matter 19:558
14. Romanovskii YV, Gerhard A, Schweitzer B, Scherf U, Personov RI, Bässler H (2000) Phys Rev Lett 84:1027
15. Sonntag M, Strohriegl P (2006) Tetrahedron 62:8103
16. Wakin S, Bouchard J, Blouin N, Michaud A, Leclerc M (2004) Org Lett 6:3414
17. Belletête M, Durocher G, Hamel S, Côte M, Wakim S, Leclerc M (2005) J Chem Phys 122:104303
18. Belletête M, Blouin N, Boudreault P-L, Leclerc M, Durocher G (2006) J Phys Chem A 110:13696
19. Belletête M, Wakim S, Leclerc M, Durocher G (2006) J Mol Struct THEOCHEM 760:147
20. Poolmee P, Ehara M, Hannongbua S, Nakatsuji H (2005) Polymer 46:6474
21. Saha B, Ehara M, Nakatsuji H (2007) J Phys Chem. A 111:5473
22. Poolmee P, Hannongbua S (2010) J Comp Chem 31:1945
23. Lu Y, Ehara M (2009) Theor Chem Acc 124:395
24. Promkatkaew M, Suramitr S, Monhaphda TK, Namuangrukd S, Ehara M, Hannongbua S (2009) J Chem Phys 131:2243060
25. Nakatsuji H, Hirao K (1978) J Chem Phys 68:2053
26. Nakatsuji H (1978) Chem Phys Lett 59:362
27. Nakatsuji H (1979) Chem Phys Lett 67:329, 334
28. Nakatsuji H (1997) SAC-CI method: theoretical aspects and some recent topics, in computational chemistry, review of current trends. World Scientific, Singapore
29. Ehara M, Hasegawa J, Nakatsuji H (2005) SAC-CI method applied to molecular spectroscopy, in theory and applications of computational chemistry: the first 40 years. Elsevier, Oxford
30. Becke AD (1988) Phys Rev A 38:3098
31. Lee C, Yang W, Parr RG (1988) Phys Rev B 37:785
32. Foresman JB, Head-Gordon H, Pople JA (1992) J Phys Chem 96:135
33. Hariharan PC, Pople JA (1973) Theo Chim Acta 28:213

34. Fukuda R, Nakatsuji H (2008) J Chem Phys 128:094105
35. Dunning Jr TH, Hay PJ (1976) In: Schaefer HF III (ed) Modern theoretical chemistry, vol 3. Plenum, New York
36. Nakatsuji H (1983) Chem Phys 75:425
37. Frisch MJ et al (2010) GAUSSIAN09 Rev. B.01. Gaussian Inc., Wallingford
38. Worth GA, Beck MH, Jackle A, Meyer H-D (2003) The MCTDH package, version 8.3. University Heidelberg, Heidelberg
39. Brière JF, Côtè M (2004) J Phys Chem B 108:3123
40. Morin J-F, Beaupré S, Leclerc M, Lévesque I, D'lorio M (2002) Appl Phys Lett 80:341
41. Blouin N, Michaud A, Wakim S, Boudreault PLT, Leclerc M, Vercelli B, Zecchin S, Zotti G (2006) Macromol Chem Phys 207:166